







PAPER

[View Article Online](#)
[View Journal](#) | [View Issue](#)Cite this: *Nanoscale*, 2025, **17**, 1411

Contactless manufacturing of TERS-active AFM tips by bipolar electrodeposition†

Yuhan Huang,  David Talaga, Gerardo Salinas,  Patrick Garrigue, Gary S. Cooney,  Stéphane Reculosa, Alexander Kuhn,  Sébastien Bonhommeau * and Laurent Bouffier *

Tip-enhanced Raman spectroscopy (TERS) is a powerful technique for nanoscale chemical imaging. However, its worldwide expansion is still limited by the challenging fabrication of cheap, robust and efficient TERS tips as optical nanosources to amplify the Raman signal. An original method based on bipolar electrodeposition is described here to prepare gold-coated AFM cantilevers used as TERS tips. This wireless method is simple to implement, cost-effective, and allows for the parallel fabrication of several TERS tips with good reproducibility of the metal thickness and a relatively long lifetime. The TERS activity was confirmed by imaging graphene oxide flakes with high spatial resolution (below 10 nm). A promising yield of 64% was achieved for the fabrication of active TERS tips. Therefore, this method could pave the way for the development of new chemical routes for the preparation of TERS tips and other plasmonic nanostructures.

Received 24th July 2024,
Accepted 6th November 2024

DOI: 10.1039/d4nr03068k

rsc.li/nanoscale

Introduction

Tip-enhanced Raman spectroscopy (TERS) has proved to be a powerful technique for nanoscale chemical and structural imaging on various nanomaterials.¹ In TERS, a scanning probe microscope (SPM), either an atomic force microscope (AFM) or a scanning tunnelling microscope (STM), is optically coupled to a Raman microscope. This cutting-edge system confers the high spatial (lateral) resolution to the TERS technique by light excitation of the localized surface plasmon resonance (LSPR) of the metal SPM probe. The global expansion of TERS as a common characterization technique is however facing the major challenge of producing in a simple, cheap and reliable way, TERS-active SPM probes (known as TERS tips). Many fabrication methods have been proposed in the literature to fabricate TERS tips,² but there is no scientific consensus on the ideal one so far. Micro- and nanofabrication methods are quite efficient to manufacture them in a reproducible way, but they are very expensive and require specific expertise. The attachment or chemical coating of noble metal nanoparticles on SPM probes is more cost-effective, but still requires technical skills in colloidal chemistry to allow nanoparticles to be placed precisely at the probe tip apex. Physical

vapor deposition methods, such as thermal evaporation and sputtering, are the most widespread techniques to fabricate TERS tips by metallization of SPM probes. However, the robustness and efficiency of the resulting probes can vary greatly. Several companies also offer TERS tips, but the cost is rather prohibitive and their efficiency is quite variable too. With respect to the aforementioned preparation methods, electrochemistry is a promising alternative. It has several key advantages, such as the simplicity of the process, which does not require specific facilities such as the access to a clean room and/or expensive equipment. STM-TERS tips are often prepared by electrochemical etching of a silver or gold wire using a simple potential step or multiple pulses.³ In contrast, AFM-TERS tips are manufactured by metallizing the AFM cantilever that is localized on a chip.^{4,5} Experimentally, the electrochemical deposition of a thin metal layer can be performed inside a cost-effective homemade electrochemical cell comprising a set of electrodes that are connected to a power supply (*i.e.* typically a potentiostat or a galvanostat depending on whether the electrodeposition is enabled according to a potential step or with a controlled current). Unfortunately, these electrochemical approaches also have several drawbacks. In most cases, the electrodeposition at the nanoscale apex of an AFM probe has a poor reproducibility due the lack of control over key parameters, such as the immersion depth inside the electrolyte. Most importantly, although AFM probes are very fragile, the manufacturing of TERS tips requires a delicate handling of AFM cantilevers through a proper connection to the power supply, achieved by using a suitable holder, some

Univ. Bordeaux, CNRS, Bordeaux INP, ISM, UMR 5255, F-33400 Talence, France.

E-mail: sebastien.bonhommeau@u-bordeaux.fr, laurent.bouffier@cnrs.fr†Electronic supplementary information (ESI) available: Experimental details, SEM characterization, EDX analysis, TERS spectra and TERS mapping. See DOI: <https://doi.org/10.1039/d4nr03068k>

copper tab or tin welding to an electrical wire. Irreversible damage to the tip can potentially occur at each step. In addition, the reproducibility of the electrodeposition process can be affected by tiny changes in the wetting proficiency inside the electrolyte, the exact positioning of the AFM chip with respect to the counter-electrode or the natural convection inside the electrochemical cell,⁵ even though a reasonable reproducibility has been reported using pulsed electrodeposition.⁴ Thus, there is still a necessity to develop an affordable and reproducible method accessible to a large number of users to fabricate TERS tips, and especially AFM-TERS tips since AFM has broader areas of application than STM.

Bipolar electrochemistry (BPE) is an unconventional electrochemical approach offering the possibility to tackle such a challenge. BPE takes place when a conducting or semiconducting substrate is immersed inside an electrolyte and subjected to an electric field.⁶ In this configuration, an interfacial potential polarization is established along the substrate enabling a driving force gradient with a maximum polarization at both extremities. The anodic polarization is obtained at the side facing the feeder cathode while a cathodic pole is established at the edge in front of the driving anode (Fig. 1a). The application of a sufficient electric field above a thermodynamic threshold value makes it possible to couple faradaic reactions across the substrate, which behaves like a so-called bipolar electrode. In other words, BPE is a contactless method that allows wireless electrochemical processes to be performed. One key application of BPE is the fabrication of dissymmetric particles,⁷ and surface gradients.⁸

In the past, BPE was already identified as a method of choice for the preparation of surface-enhanced Raman spectroscopy (SERS)-active substrates,^{9–11} allowing for molecular sensing, provided that the LSPR of substrate metal nanoparticles is conveniently excited by laser light, like in TERS. An Ag–Au alloy gradient was deposited on a stainless-steel substrate using BPE prior to a post-modification by grafting a benzene thiol self-assembled monolayer. Monitoring of the

SERS response alongside the bimetallic gradient allowed the determination of the optimum alloy composition that maximized the signal.⁹ Moreover, by selecting another monolayer containing an electroactive moiety such as quinone/hydroquinone redox couple, SERS was also recorded under electrochemical control along the bipolar electrode.¹¹ The use of electrochemical SERS and BPE was found to be very appropriate for probing the local potential distribution of solid-state nanopores.¹² The authors demonstrated that the SERS signal from the redox-active Nile Blue A dye was self-consistent with the variation of polarizations on the gold nanopores. Finally, BPE fabrication of a size gradient of truncated spherical Au nanovoids was reported. The idea was to screen and identify the most efficient SERS-active structure alongside the bipolar electrode. The highest enhancement was obtained for a particular nanovoid dimension having a diameter of 260 nm.¹³ Once again in this example, the key discovery was to use the electrochemical driving force gradient alongside the bipolar electrode in order to screen various electrodeposition conditions.

Despite these previous reports on SERS applications, BPE has never been employed for the electrochemical fabrication of TERS tips. In this contribution, we will demonstrate the key advantage of such a wireless approach to manufacture multiple AFM-TERS tips with good reproducibility, not only to record TERS spectra but also to collect reliable TERS maps with nanoscale spatial resolution.

Experimental

Pre-treatment of AFM chips

Prior to metal deposition, n-doped silicon AFM chips (ACCESS-FM, AppNano) were immersed for 2 min in 5% HF aqueous solution (prepared after dilution of a 48% v/v HF solution in water from Sigma-Aldrich, 99.99%). Subsequently, the chips were rinsed thoroughly with ultrapure (Milli-Q®) water and dried under a gentle N₂ gas flow.

TERS tip preparation

The freshly etched AFM chips were simply immersed in the plating electrolyte within the electrochemical cell, and placed parallel to each other but perpendicular to the two feeder electrodes, with the AFM cantilevers (and thus the AFM tips at their ends) facing the feeder anode. A 6.9 V cm^{−1} electric field was applied between the 2 feeder electrodes for 5 s to 15 s. Once the bipolar electrodeposition process was completed, the TERS tips were rinsed 3 times with Milli-Q® water and dried under a gentle N₂ gas flow. After preparation, the TERS tips were stored in Argon (99.9999% purity) until use for TERS experiments.

TERS experiments

TERS measurements were conducted using a side-illumination NanoRaman system (HR Evo Nano, HORIBA Scientific), which comprises an Omegascope atomic force microscope combined

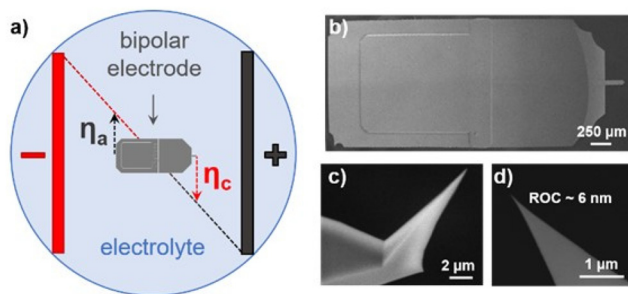


Fig. 1 (a) Diagram of a bipolar electrochemistry setup with the n-doped silicon AFM chip used as bipolar electrode (not to scale). The red and black electrodes are the driving cathode and anode, respectively. η_a and η_c indicate the anodic and cathodic overpotentials localized at the extremities of the bipolar electrode. SEM images recorded at various magnifications displaying a top view of the 3645 μm -long gold-coated chip (b), a tilted view of the end of a pristine cantilever (c), and the apex of the corresponding tip (d).

with a LabRAM HR Evolution Raman spectrometer. Linearly polarized laser light (633 nm, 170 μW) was used to irradiate the sample surface through a 100 \times objective (MITUTOYO, 0.7 NA). All TERS spectra were acquired using a 600 grooves per mm diffraction grating. All TERS maps were carried out in the hybrid contact mode developed by HORIBA (applied force ~ 1 nN). In this specific mode, the TERS tip is in contact with the sample surface only during the acquisition of the TERS signal. The sample probed by TERS was a test sample purchased from HORIBA which contained graphene oxide (GO) sheets and carbon nanotubes deposited on a gold-coated substrate. TERS spectra were slightly smoothened using the Savitzky–Golay algorithm and a baseline correction based on a 5th degree polynomial (LabSpec 6 software).

Scanning electron microscopy

A Tescan Vega 3 SEM equipped with a Bruker XFlash 630M energy dispersive X-ray (EDX) spectroscopy detector was used to perform SEM imaging at 10 mm working distance and 15 kV acceleration voltage, as well as the elemental analysis of AFM tip coatings.

Results and discussion

The principle of the developed BPE method is displayed in Fig. 1a in the case of a single n-doped silicon AFM chip as bipolar electrode, immersed inside the electrolyte and positioned in between two feeder electrodes. These later electrodes are commercially available platinum-coated glass slides separated by a 1.6 cm distance. The volume of the electrolyte is typically 2.5 mL. Notably, the AFM chip is directly immersed without any holder or fixation, a contactless setup that minimizes contamination risk from external supports during electrodeposition process. The AFM probe chip (length \times width \times thickness = 3400 μm \times 1600 μm \times 315 μm) carries a 245 μm -long cantilever (Fig. 1b), at the end of which a 10 μm -long tip with a 6 nm radius of curvature (ROC) apex protrudes (Fig. 1c and d). The AFM chip is oriented perpendicular to the feeder electrodes, with the tip facing the feeder anode so that it can act as a local cathodic pole during BPE.

During BPE, two electrochemical reactions are coupled and take place at the two opposite sides of the bipolar electrode under the influence of the applied electric field. Prior to BPE, the n-doped Si AFM tip should be etched in HF solution so that the unavoidable SiO_2 thin layer on Si in air can be readily dissolved (see experimental details). The extrinsic conductivity of the n-doped Si is then sufficient to ensure electron transfer without photoexcitation, just like a metal conductor rather than a semiconductor. For the sake of reproducibility and repeatability in other laboratories, we deliberately chose to employ a commercially available gold sulfite plating solution, which is known to afford regular gold layers on flat surfaces together with sufficient ionic conductivity.¹⁴ The electrochemical reaction that takes place at the cathodic pole is the reduction of the gold precursor, which is the $[\text{Au}(\text{SO}_3)_2]^{3-}$

anion. On the other hand, several oxidation reactions can take place at the anodic domain depending on the driving force, but the easiest ones are the oxidations of Si and of water. This means that the minimal polarization voltage established across the bipolar electrode should be equal to several hundreds of mV based on the corresponding standard potentials (Table S1 in ESI[†]). However, in practice, we observed that the electric field necessary to promote substantial electrodeposition was typically above 6 V cm^{-1} , corresponding to a theoretical polarization of about 2.4 V on the 3.6 mm long Si chip when its main axis of symmetry is oriented parallel to the electric field lines. Such a large overpotential reflects the non-linearity of the voltage drop throughout the electrolyte, and is commonly observed during BPE in an open-configuration cell.^{7,15} SEM images reported in Fig. 2 provide a comparison of a tip apex before (Fig. 2a), and after BPE for 10 s when applying an electric field of 6.9 V cm^{-1} (Fig. 2b). These images clearly demonstrate that a thin gold layer was effectively deposited on the Si tip, as illustrated by the overlaid images displayed in Fig. 2c. Interestingly, the value of the applied electric field is sufficient to coat with gold about 15% of the AFM chip, as shown in Fig. 1b on which a ~ 500 μm -long metal deposit is clearly visible by optical contrast (shiny region on the right-hand side). Beyond this first proof-of-principle experiment, tuning the electric field strength should allow either the deposit to be concentrated at the extremity of the tip or, on the contrary, the zone of deposition to be extended over a larger portion of the cantilever.

A confirmation of the nature of the metal deposit was obtained by carrying out energy dispersive X-ray (EDX) analysis of two distinct zones at the two ends of an AFM chip (Fig. S1a[†]). In the absence of any visible deposit at the bottom of the AFM chip, only the signal assigned to Si was observed at 1.76 keV (Fig. S1b[†]). However, on the opposite side, the signal of gold pointing at 1.94 keV was clearly recorded on the tip cantilever, in addition to the Si contribution (Fig. S1c[†]).

The influence of the electrodeposition time was studied in order to demonstrate that the thickness of the gold layer can be readily controlled. Three AFM chips were coated with gold by applying an electric field of 6.9 V cm^{-1} for 5 s, 10 s and 15 s, respectively (Table S2[†]). Their SEM characterization revealed that the amount of deposited gold is gradually increased with time. The thickness of the gold layer can be assessed from the apparent ROC of the TERS tip apex. The ROC measured for a

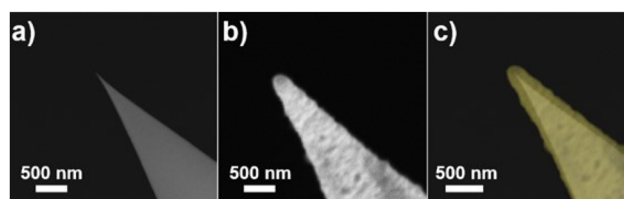


Fig. 2 SEM images of the Si tip apex (a) before gold electrodeposition, and (b) after gold electrodeposition (electric field: 6.9 V cm^{-1} ; electrodeposition time: 10 s), together with (c) their colour-enhanced overlay.

5 s deposition was estimated at 90 nm, and this value was found to double for a 15 s deposition (ROC \sim 180 nm). It is noteworthy that such large ROC values are compatible with TERS activity, and do not modify necessarily the TERS enhancement and the electromagnetic confinement at the origin of the high spatial resolution of TERS. In a non-gap-mode TERS configuration (for which the sample is placed on an insulating substrate and/or the tip–substrate distance is larger than 2–5 nm), the TERS enhancement and the resolution are expected to decrease with the increased size of the tip apex,¹⁶ but they also strongly depend on the presence of nano-scale protrusions at the very end of the tip.^{5,17} The fine control of the thickness of the gold deposit confirms that BPE is indeed a method of choice to fabricate TERS tips.

Besides the electrodeposition time, the parallel fabrication of TERS tips constitutes a critical aspect to make BPE more appealing for the TERS community. Standard potentiostatic electrodeposition necessitates manufacturing these tips once at a time. Such a limitation can be circumvented since BPE is a contactless method. The parallel electrodeposition of three AFM chips was performed by immersing them side by side in the same electrochemical cell filled with gold plating solution. Within our small electrochemical cell (3.4 cm in diameter), AFM chips were spaced by a few millimetres (\sim 5 mm), and felt the same homogeneous electric field distribution, resulting in similar gold thicknesses at their surface (Table S3†). Simultaneous gold bipolar electrodeposition on five tips have been also performed occasionally, with similar quality of the metal layer. The scale-up of the electrochemical cell should be quite straightforward (with appropriate dimensions of the electrochemical cell to maintain a homogeneous electric field distribution), and allow the parallel fabrication of many more TERS tips.

To estimate the activity of the TERS tips, AFM-TERS was conducted under 633 nm irradiation on a commercial graphene oxide/carbon nanotube sample deposited on a gold-coated substrate (see experimental details). The 633 nm wavelength is indeed suitable to excite the LSPR of gold TERS tips.^{18,19} In our experimental conditions, TERS tips fabricated with an electric field of 6.9 V cm^{-1} for 5 s electrodeposition time were chosen for testing, as the ones with 10 s and 15 s electrodeposition times exhibited a larger size of tip apexes ($>135 \text{ nm}$), which would impede the AFM image quality. It is noteworthy that these conditions were also the best trade-off to obtain a homogeneous gold coating and a relatively small tip apex ROC to prevent any strong deterioration of the lateral resolution in AFM imaging (Fig. S2†). Considering these experimental electrodeposition parameters, 64% of the TERS tips (7 out of 11 tips) produced by BPE showed a TERS efficiency sufficient to collect TERS spectra. This constitutes an improvement compared to the 53% fabrication yield reported for some potentiostatic methods,⁵ and the \sim 60% yield of metal sputtering.²⁰ This 64% yield is a reasonable value considering the cost-effectiveness and simplicity of the bipolar electrodeposition method, and offers a practical alternative to expensive micro- and nano-fabrication techniques with higher fabrication yield.^{2,21}

Fig. 3a shows an AFM image alongside four TERS maps, acquired using a single TERS tip (TERS measurements with additional tips are provided in Fig. S3–S5†). The region imaged in Fig. 3a is only a small portion of a larger graphene oxide (GO) flake (Fig. S6†). The cyan and green TERS images were obtained through integration of the intensity within the $1220\text{--}1420 \text{ cm}^{-1}$ and $1520\text{--}1660 \text{ cm}^{-1}$ range, respectively, which encompass the characteristic marker bands of GO, namely the D band, situated around 1350 cm^{-1} , and the G band, at approximately 1580 cm^{-1} (Fig. 3b). The TERS signal exhibits relatively homogeneous intensity across the GO flake regions, rather than being more intense at the GO edges and steps, as already reported for graphene^{18,22} and GO.^{18,19} This is seemingly due to the presence of folds and wrinkles (Fig. S6†). Unlike flat GO sheets, these disordered structures introduce defects that can enhance the TERS signal, resulting in a more uniform distribution within the dotted-line region. This increased TERS signal should arise from the better alignment of the axially polarized near-field component with the Raman polarizability tensor components involved in GO vibrations, in regions where the GO lattice is somewhat disrupted.¹⁹ The AFM topographical images in Fig. 3a and 4a suggest the GO to be multi-layered and much thicker than

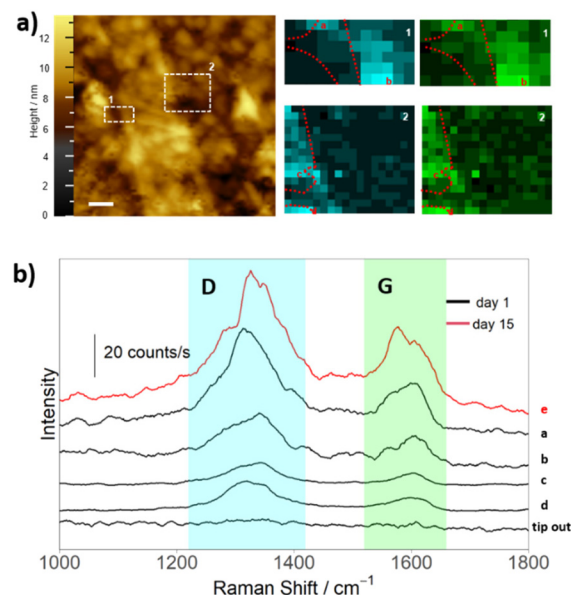


Fig. 3 (a) Left: Tapping-mode topographical AFM image of a part of GO flake scanned by a TERS tip. Scale bar: 100 nm. Right: Two TERS maps corresponding to the white dotted boxes in the AFM image. The red dotted lines indicate the edge of a GO flake within a multilayer structure. Spectral range for intensity integration: cyan D band: $1220\text{--}1420 \text{ cm}^{-1}$, green G band: $1520\text{--}1660 \text{ cm}^{-1}$; scanning step size: 10 nm; acquisition time: (1) 3 s, (2) 5 s. (b) Black spectra (obtained on day 1): TERS spectra a–d measured at the positions marked with red a–d labels in TERS maps 1 and 2. The tip-out spectrum illustrates the TERS spectrum obtained when the tip is retracted from the sample surface. Red spectrum: TERS spectrum e recorded using the same TERS tip two weeks after (day 15) fabrication (storage under Ar) when the tip is engaged on the sample surface.

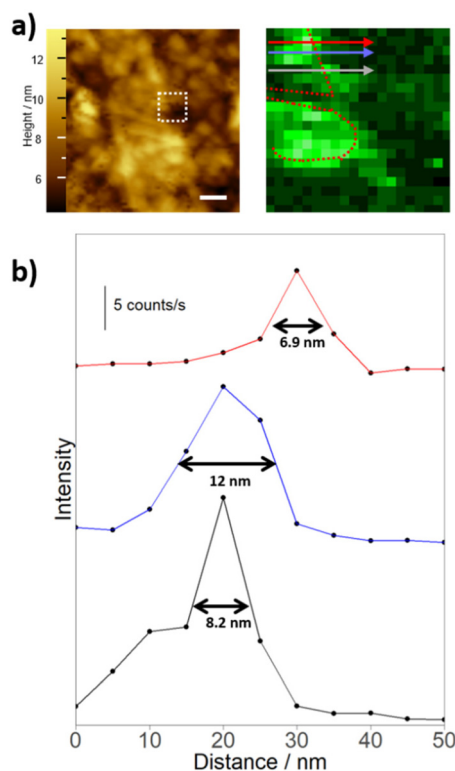


Fig. 4 (a) Left: Tapping-mode topographic AFM image of a part of GO flake scanned by a TERS tip. Scale bar: 100 nm. Right: TERS map bounded by the white dotted square box in the AFM image. The red dotted lines indicate the edge of a GO flake within a multilayer structure. Spectral range for intensity integration: 1200–1670 cm^{-1} ; scanning step size: 5 nm, acquisition time: 5 s. (b) Three TERS intensity profiles along the arrows drawn in (a), with their corresponding full width at half maximum. Band for intensity integration: 1350 cm^{-1} .

1–5 nm, which implies a limited gap-mode enhancement, or a weak effect of the gold-coated substrate on the TERS enhancement.^{1,23} The observed TERS enhancement seems to be largely due to the tip itself.

Fig. 4 presents another TERS map from the same sample area as in Fig. 3a, that was obtained by integrating the TERS signal over the 1200–1670 cm^{-1} spectral range. Three TERS intensity profiles obtained by intensity integration of the D band at 1350 cm^{-1} along arrows indicated in the TERS map are also provided. They show full widths at half maximum between 6.9 and 12 nm, which suggests that TERS imaging was performed with a spatial resolution better than 10 nm. This value is much smaller than the radius of curvature of the tip apex (~ 100 nm in this case), and is consistent with the electron confinement in a nanoscale gold protrusion at the extremity of the tip apex.¹⁷ Moreover, this is in line with the resolution achieved in similar samples using gold-coated tips.¹⁹

The lifetime of TERS tips is also an important criterion to consider them reliable for characterization by TERS. It is prone to vary from hours to months depending on the robustness of the metal coating, TERS imaging parameters, as well as environmental conditions.^{23,24} In Fig. 3b, spectra a–d display

TERS spectra at marked positions a–d in TERS maps 1 and 2. A large enhancement of the GO D and G bands is observed when the tip is engaged on the GO surface, but no signal can be discerned when the tip is retracted 18 μm above the GO surface (tip-out spectrum). Two weeks later, a TERS spectrum can still be discerned using the very same tip (red spectrum e), provided that it was stored under Ar atmosphere until use. This tip thus remained TERS-active during measurements on day 1 and day 15, after a TERS mapping time of nearly 7 hours, which is sufficient for most TERS imaging experiments. This suggests that tips prepared by bipolar electrodeposition are quite stable in time due to the inertness of gold, and robust enough to withstand day-long TERS imaging periods.

Conclusions

An original wireless BPE method was used for the parallel preparation of gold-coated AFM-TERS tips with good reproducibility of the metal thickness and a satisfying fabrication yield (64%). Since the approach is contactless, it significantly prevents possible mechanical damage due to the wiring step necessary when employing more conventional electrodeposition approaches. This fast, inexpensive and easy fabrication method led to good TERS activities and relatively long lifetimes of the TERS probes, which proved to be quite robust. These AFM chips were not only TERS-active but were also successfully used to perform TERS mapping. It turned out that they were appropriate to perform TERS imaging in air with high spatial resolution (below 10 nm). This original method is easy to implement anticipating the rapid opening of new perspectives for the design of optical nanosources for TERS and beyond.

Author contributions

Yuhan Huang: Methodology, investigation, formal analysis, validation, visualization, writing – original draft; David Talaga: Investigation; Gerardo Salinas: Investigation; Patrick Garrigue: Investigation; Gary S. Cooney: Investigation; Alexander Kuhn: Funding acquisition, methodology; Sébastien Bonhommeau: Conceptualization, funding acquisition, methodology, project administration, supervision, writing – original draft; Laurent Bouffier: Conceptualization, methodology, supervision, writing – original draft.

Data availability

Data for this article, including SEM images, TERS spectra and TERS mapping are available at <https://sdrive.cnrs.fr/s/x7HwLBMnoFHPp5Y>. N.B. from the authors: this URL is provided by the French employer (CNRS) and it will be updated prior to online publication of the manuscript.

Conflicts of interest

There are no conflicts to declare.

Note added after first publication

This article replaces the version published on 8th November 2024, which contains an updated link to access the data for this article, including SEM images, TERS spectra and TERS mapping.

Acknowledgements

The PhD scholarship of YH was funded by the Agence Nationale de la Recherche under contract no. ANR-20-CE29-0004 (AQUATERS). The PhD scholarship of GSC was funded by the University of Bordeaux. AK and GS acknowledge financial support by the European Research Council (ERC, Advanced Grant ELECTRA) under the European Union's Horizon 2020 research and innovation program (grant agreement no. 741251). TERS measurements were performed at the platform SIV (Spectroscopie et Imagerie Vibrationnelle) funded by the European Union (FEDER), the Région Nouvelle Aquitaine and the University of Bordeaux.

References

- 1 P. Pienpinijtham, Y. Kitahama and Y. Ozaki, *Nanoscale*, 2022, **14**, 5265; S. Bonhommeau, G. S. Cooney and Y. Huang, *Chem. Soc. Rev.*, 2022, **51**, 2416.
- 2 X. Shi, N. Coca-Lopez, J. Janik and A. Hartschuh, *Chem. Rev.*, 2017, **117**, 4945; S. Bonhommeau and S. Lecomte, *ChemPhysChem*, 2018, **19**, 8.
- 3 B. Ren, G. Picardi and B. Pettinger, *Rev. Sci. Instrum.*, 2004, **75**, 837; T. W. Huh, G. Han, W. J. Ban and H. S. Han, *Int. J. Precis. Eng. Manuf.*, 2017, **18**, 221.
- 4 L.-K. Yang, T.-X. Huang, Z.-C. Zeng, M.-H. Li, X. Wang, F.-Z. Yang and B. Ren, *Nanoscale*, 2015, **7**, 18225; T.-X. Huang, C.-W. Li, L.-K. Yang, J.-F. Zhu, X. Yao, C. Liu, K.-Q. Lin, Z.-C. Zeng, S.-S. Wu, X. Wang, F.-Z. Yang and B. Ren, *Nanoscale*, 2018, **10**, 4398.
- 5 Y. Huang, D. Talaga, P. Garrigue, G. Salinas, G. S. Cooney, S. Reculosa, A. Kuhn, L. Bouffier and S. Bonhommeau, *Chem. Phys. Lett.*, 2023, **832**, 140893.
- 6 N. Shida, Y. Zhou and S. Inagi, *Acc. Chem. Res.*, 2019, **52**, 2598; N. Karimian, P. Hashemi, A. Afkhami and H. Bagheri, *Curr. Opin. Electrochem.*, 2019, **17**, 30; K. L. Rahn and R. K. Anand, *Anal. Chem.*, 2021, **93**, 103; Y.-L. Wang, J.-T. Cao and Y.-M. Liu, *ChemistryOpen*, 2022, **11**, e202200163; G. Salinas, S. Arnaboldi, L. Bouffier and A. Kuhn, *ChemElectroChem*, 2022, **9**, e202101234.
- 7 J.-C. Bradley and Z. Ma, *Angew. Chem., Int. Ed.*, 1999, **38**, 1663; C. Warakulwit, T. Nguyen, J. Majimel, M.-H. Delville, V. Lapeyre, P. Garrigue, V. Ravaine, J. Limtrakul and A. Kuhn, *Nano Lett.*, 2008, **8**, 500; Y. Koizumi, N. Shida, I. Tomita and S. Inagi, *Chem. Lett.*, 2014, **43**, 1245; I. Malytska, T. Doneux, M. Bougouma, A. Kuhn and L. Bouffier, *J. Phys. Chem. C*, 2019, **123**, 5647; P. Chassagne, P. Garrigue and A. Kuhn, *Adv. Mater.*, 2023, **36**, 2307539.
- 8 C. Ulrich, O. Andersson, L. Nyholm and F. Björefors, *Angew. Chem., Int. Ed.*, 2008, **47**, 3034; S. Inagi, Y. Ishiguro, M. Atobe and T. Fuchigami, *Angew. Chem., Int. Ed.*, 2010, **49**, 10136; S. Ramakrishnan and C. Shannon, *Langmuir*, 2010, **26**, 4602; N. Shida, Y. Koizumi, H. Nishiyama, I. Tomita and S. Inagi, *Angew. Chem., Int. Ed.*, 2015, **54**, 3922; H. Termebaf, M. Shayan and A. Kiani, *Langmuir*, 2015, **31**, 13238; A. Lundgren, S. Munktell, M. Lacey, M. Berglin and F. Björefors, *ChemElectroChem*, 2016, **3**, 378; L. Bouffier, S. Reculosa, V. Ravaine and A. Kuhn, *ChemPhysChem*, 2017, **18**, 2637.
- 9 R. Ramaswamy and C. Shannon, *Langmuir*, 2011, **27**, 878.
- 10 A. Sanghapi, S. Ramakrishnan, S. Fan and C. Shannon, *ChemElectroChem*, 2016, **3**, 436.
- 11 B. Wang, S. Yu and C. Shannon, *ChemElectroChem*, 2020, **7**, 2236.
- 12 Y. Li, C. Chen, K. Willems, S. Kerman, L. Lagae, G. Groeseneken, T. Stakenborg and P. Van Dorpe, *Adv. Opt. Mater.*, 2017, **5**, 1600907.
- 13 Y. U. Kayran, V. Eßmann, S. Grütze and W. Schuhmann, *ChemElectroChem*, 2016, **3**, 399.
- 14 S. H. Pu, A. S. Holmes and E. M. Yeatman, *Microelectron. Eng.*, 2013, **112**, 21.
- 15 Z. Fattah, G. Loget, V. Lapeyre, P. Garrigue, C. Warakulwit, J. Limtrakul, L. Bouffier and A. Kuhn, *Electrochim. Acta*, 2011, **56**, 10562.
- 16 T. Huang, S. Huang, M. Li, Z. Zeng, X. Wang and B. Ren, *Anal. Bioanal. Chem.*, 2015, **407**, 8177.
- 17 S. Trautmann, M. Richard-Lacroix, A. Dathe, H. Schneidewind, J. Dellith, W. Fritzsche and V. Deckert, *Nanoscale*, 2018, **10**, 9830.
- 18 A. Bhattarai, A. Krayev, A. Temiryazev, D. Evplov, K. T. Krampton, W. P. Hess and P. Z. El-Khoury, *Nano Lett.*, 2018, **18**, 4029.
- 19 W. Su, N. Kumar, A. Krayev and M. Chaigneau, *Nat. Commun.*, 2018, **9**, 2891.
- 20 S. Bonhommeau, D. Talaga, J. Hunel, C. Cullin and S. Lecomte, *Angew. Chem., Int. Ed.*, 2017, **56**, 1771.
- 21 T. W. Johnson, Z. J. Lapin, R. Beams, N. C. Lindquist, S. G. Rodrigo, L. Novotny and S.-H. Oh, *ACS Nano*, 2012, **6**, 9168–9174.
- 22 M. Ghislandi, G. G. Hoffmann, E. Tkalya, L. Xue and G. D. With, *Appl. Spectrosc. Rev.*, 2012, **47**, 371.
- 23 Z. Zhang, S. Sheng, R. Wang and M. Sun, *Anal. Chem.*, 2016, **88**, 9328.
- 24 B. S. Yeo, J. Stadler, T. Schmid, R. Zenobi and W. Zhang, *Chem. Phys. Lett.*, 2009, **472**, 1; N. Kumar, S. J. Spencer, D. Imbraguglio, A. M. Rossi, A. J. Wain, B. M. Weckhuysen and D. Roy, *Phys. Chem. Chem. Phys.*, 2016, **18**, 13710.